

Traction Between a Web and a Smooth Roller

Sinan Müftü

Associate Professor, Member ASME

John J. Jagodnik,

Graduate Student

Northeastern University

Department of Mechanical Engineering

Boston, MA 02115

Submitted for review in Journal of Tribology, Transactions of the ASME

July 2002

Abstract

Web traction over rollers is known to deteriorate due to air entrainment at high web speeds. In this paper, a general model is presented to predict the traction capability of an impermeable web over a smooth roller. The model considers the effects of the web and roller speeds, roller radius, combined roughness of the two surfaces, web tension and thickness, friction coefficient, and compressible air bearing. The change of tension ΔN due to mechanical slip between the roller and the web is calculated by a simultaneous solution of the in-plane and out-of-plane equilibrium of the web. The problem is non-dimensionalized and the effects of nine of the eleven non-dimensional parameters on traction are investigated for a range of values. Formulas involving the non-dimensional parameters for the traction capability are presented in two variable polynomial forms.

Introduction

Thin, flexible, continuous sheets such as magnetic recording tape, paper, textiles and various forms of film are generally called webs. Web handling operations involve translation of a tensioned web over and under rollers, driers, coating and calendering stations, depending on the application. In web handling systems, rollers are one of the most common guiding elements. The function of a roller is to guide the web without changing its tension. This is possible if good traction exists between the web and the roller. However, web traction over rollers is known to deteriorate due to air entrainment at high web speeds [1,2]. In this paper, a general model is presented to predict the traction capability of an impermeable web over a smooth roller.

A web guided by an ideal roller without any bearing resistance, operating in vacuum should not experience any slip over the roller, if the friction coefficient between the web and the roller is greater than zero [3]. However, some amount of air entrainment in the web roller interface is unavoidable in practice. The entrained air layer causes *mixed lubrication* condition to develop in the web-roller interface, where the web is supported partially by the rigid body contact of the asperities, and partially by the air layer which has a super ambient pressure level. The mechanics of a web interacting with a self-acting air lubrication layer is described by the *foil bearing* problem, which excludes the contact conditions [4-8]. Mixed lubrication in foil bearing problem has been investigated by [9-12].

In the case of mixed lubrication in the web roller interface, the belt-wrap pressure, T/R_r , is balanced partially by rigid body contact between the asperities and partially by air pressure. With increasing web speed, the amount of entrained air and consequently the magnitude of air pressure increases. This results in a smaller portion of the belt-wrap pressure to be shared by the rigid body contact pressure. Thus one can see, by considering Coulomb's friction law, $F_f = \mu F_n$, that the frictional force required to sustain high traction can be effectively reduced, without altering the value of the coefficient of static friction, μ .

It is possible for the web to lose contact with the roller as a result of air entrainment. However, it should be noted that, in practice, this is unlikely; as the web starts to fly, the contribution of the roller to entrain air will decrease; and the web will contact the roller, again. If the web operating conditions are not adjusted, web will chatter over the roller, causing transient tension changes and web scratches.

Ducotey and Good developed an algorithm for predicting web traction over smooth rollers [1]. They added modifications to the classical foil bearing theory to accommodate the effects of web permeability, side air leakage and surface roughness. Results were favorable when compared to their experiments. They concluded that an increase in surface roughness significantly increases traction. Ducotey and Good also modeled grooved rollers where they showed that using circumferentially placed grooves on a roller can improve the traction characteristics [13]. Rice et al. introduced a model for determining the effective asperity height for a variety of surface characteristics in the web-roller interface [2]. They modeled the web as an Euler-Bernoulli beam; used the compressible Reynolds lubrication equation to model the air entrainment effects; and included an asperity compliance model for contact between the web and the roller.

Experimental measurements of the traction capability of a given web-roller interface involves inducing slip at different transport speeds, by applying a breaking

torque on the roller [1,2]. At different web speeds, different breaking torque values cause slip between the web and the roller. These experiments, thus establish a functional relationship between the web speed and slipping torque value. When slip occurs, the web tension increases in the sliding direction by ΔN , which is related to the breaking torque value. The results of the experiments are typically reported by calculating an *equivalent coefficient of friction* μ_e or *traction coefficient* with the capstan formula,

$$\mu_e = \frac{1}{\beta} \ln \left(\frac{\Delta N}{T} + 1 \right) \quad (1)$$

where the inlet tension is T and the wrap angle is β [1,2]. Note that in these experiments, a small ΔN indicates weak traction capability of the interface.

Traction loss primarily depends on the web speed. However, roller radius, combined roughness of the two surfaces, web tension and thickness and permeability of the web are also factors that affect traction. Effects of web or roller permeability have been studied by various authors [1,14,15]; these effects are not considered in this work. In this paper, a model for the traction measurements as described in the above paragraph is introduced. The change of tension ΔN due to slip is calculated by considering the equilibrium of the in-plane stress resultant N . This is in contrast to earlier models, where ΔN is calculated from $\Delta N = \mu_s F_n / (T / R_r)$ [2,13]. Nine non-dimensional parameters are identified and their effects on traction are investigated for a range of values. Formulas involving the non-dimensional parameters for the traction capability are also presented.

Model of the web-roller interface

The equations of equilibrium for a web travelling over a cylindrical surface at steady state as shown in Figure 1 are given by the following coupled set of equations [15,17],

$$D \frac{d^4 w'}{dx^4} + D_s w' + (\rho c v^2 - N) \frac{d^2 w}{dx^2} - \frac{dN}{dx} \frac{dw}{dx} = (p - p_a) + p_c - \frac{N}{R(x)} \quad (2a)$$

$$\frac{dN}{dx} + \tau = 0 \quad (2b)$$

where $w' = w - w_r$ is the web deflection measured with respect to the equilibrium spacing w_r calculated for a stationary web [15]. Other variables are listed in the nomenclature. Equation (2a) represents the combined out-of-plane and moment equilibria. In particular on the left hand side of this equation, the first term represents the bending stiffness of the web; the second term represents the shell-stiffness due to the wrapping the web around a cylindrical surface; and the third and the fourth terms represent the effects of in-plane stress resultant N on the out-of-plane equilibrium. Note that the third term of the right hand side has the only remaining term of the gyroscopic accelerations at steady state $\rho c v^2 (d^2 w / dx^2)$. The right hand side of equation (2a) shows the effect of air pressure p measured with respect to the ambient pressure p_a , the rigid body contact pressure p_c , and the belt-wrap pressure $N/R(x)$. The curvature of the web is given by,

$$\frac{1}{R(x)} = \frac{1}{R_r} \left\{ e^{-\left(1 + \frac{L_1 - x}{b}\right)} [H(x) - H(x - L_1)] + [H(x - L_1) - H(x - L_2)] + e^{-\left(1 + \frac{x - L_2}{b}\right)} H(x - L_2) \right\} \quad (3)$$

where R_r is the roller radius and $b = (D/T)^{1/2}$ is the characteristic bending length of the web [17]. Tangency points of the web L_1 and L_2 are ordered as follows $0 < L_1 < L_2 < L$. Equation (2b) represents the in-plane equilibrium. In this problem, the in-plane traction τ occurs due to sliding contact. Coulomb's friction law is used to find τ as follows,

$$\tau = \mu_s p_c \begin{cases} -1 & \text{if } v > 0 \\ 1 & \text{if } v < 0 \end{cases} \quad (4)$$

where μ_s is the dynamic or the "slow-speed" friction described in reference [2]. The rigid body contact pressure is modeled using a non-linear empirical relation [2,9,18],

$$p_c = P_0 \left(1 - \frac{h}{\sigma_0} \right)^2. \quad (5)$$

The web-roller clearance h is calculated by,

$$h = w + \delta \quad (6)$$

where $\delta(x)$ is the initial clearance between the web and the roller measured normal to the roller surface as shown in Figure 1. The web is assumed to have simple supports on its boundaries,

$$\text{at } x = 0, L: w = D \frac{d^2 w}{dx^2} = 0. \quad (7)$$

The upstream tension T is specified as the boundary condition of the in-plane equilibrium equation (3b). For $v > 0$ this becomes,

$$\text{at } x = 0: N = T. \quad (8)$$

The air lubrication in the interface is modeled by using the Reynolds lubrication equation with first-order slip flow corrections. The corrections for slip flow become necessary when the web-roller clearance is in the order of the length of molecular mean free path of air λ . This equation for a compressible, ideal gas is [19],

$$\frac{d}{dx} \left[(ph^3 + 6\lambda h^2) \frac{dp}{dx} \right] = 6\mu V \frac{dph}{dx}. \quad (9)$$

On the boundaries the air pressure is set to the ambient pressure p_a . Equations (2-9) are coupled, non-linear equations. Their solution is obtained numerically as described in [14].

Non-dimensional Form of the Governing Equations

The set of equations (2-9) has one independent variable x , four dependent variables, w , p , p_c , and N and sixteen parameters that affect the dependent variables. In order to reduce the number of parameters that control the problem the following non-dimensional independent variables are defined,

$$\bar{x} = \frac{x}{L_w}, \quad \bar{w} = \frac{w}{c}, \quad \bar{h} = \frac{h}{\sigma_0}, \quad \bar{p} = \frac{p}{p_a}, \quad \bar{p}_c = \frac{p_c}{p_a}, \quad \bar{N} = \frac{N}{T} \quad (10)$$

where $L_w = \beta R_r$ is the wrap length. Substitution of these variables in the governing equations results in following eleven non-dimensional control parameters,

$$S = \frac{Ec}{T(1-v^2)}, \quad C = \frac{c}{L_w}, \quad P = \frac{p_a R_r}{T}, \quad V = \frac{v}{\sqrt{T/c\rho}}, \quad \beta = \frac{L_w}{R_r}, \quad X_L = \frac{x_L}{L_w}, \quad X_R = \frac{x_R}{L_w},$$

$$\Sigma = \frac{\sigma_0}{c}, \quad P_0 = \frac{p_0}{p_a}, \quad \Lambda = \frac{\lambda}{\sigma_0}, \quad B = \frac{6\mu_a v L_w}{p_a \sigma_0^2}. \quad (11)$$

The coefficient of friction μ_s remains unchanged. With these non-dimensional variables the governing equations become,

$$\frac{SC^2}{12} \frac{d^4 \bar{w}}{d\bar{x}^4} + S\beta^2 \bar{w}' + (V^2 - \bar{N}) \frac{d^2 \bar{w}}{d\bar{x}^2} - \frac{d\bar{N}}{d\bar{x}} \frac{d\bar{w}}{d\bar{x}} = \frac{\beta}{C} [P(\bar{p} + \bar{p}_c - 1) - \bar{N}] \quad (12a)$$

$$\frac{d\bar{N}}{d\bar{x}} + \bar{\tau} = 0 \quad (12b)$$

$$\frac{d}{d\bar{x}} \left[(\bar{p}\bar{h}^3 + 6\Lambda\bar{h}^2) \frac{d\bar{p}}{d\bar{x}} \right] = B \frac{d\bar{p}\bar{h}}{d\bar{x}} \quad (13)$$

$$\Sigma\bar{h} = \bar{w} + \bar{\delta} \quad (14)$$

$$\bar{p}_c = P_0 (1 - \bar{h})^2 \quad (15)$$

$$\bar{w}' = \bar{w} - \bar{w}_r \quad (16)$$

$$\bar{\tau} = \mu_s PC \bar{p}_c \begin{cases} -1 & \text{if } V > 0 \\ 1 & \text{if } V < 0 \end{cases} \quad (17)$$

Results

In this work, the effects of nine of the eleven non-dimensional parameters described above on the traction between a roller and a flexible web are investigated. The effect of X_L and X_R are not considered; it is reasonable to assume that by specifying these two parameters much greater than the non-dimensional bending length, b/L_w , their effect can be neglected. The change in tension at the onset of sliding $\Delta\bar{N}$ strongly depends on air entrainment; and the bearing number B controls the pressure generation to a great extent. Therefore, in investigating the effects of the non-dimensional parameters on $\Delta\bar{N}$ we paired each parameter with B , while keeping all the rest of the parameters constant. For example, we investigated $\Delta\bar{N} = f(B, C)$ and $\Delta\bar{N} = f(B, \Sigma)$, etc.

Values of the parameters for a typical tape transport are given in Table 1; the corresponding non-dimensional parameters are given in Table 2. Table 3 lists the ranges of the non-dimensional parameters used in this work. When, for example, the effects of B and S are investigated simultaneously, their values are taken from Table 3, ($14 \leq B \leq 570$ and $148 \leq S \leq 2470$), and all the rest of the parameters are kept at their base values, given in Table 2. In the numerical simulations, the B range is divided into 40 equal parts and the range of the second parameter is divided into 25 equal parts. This results in a total of one thousand parameters, to obtain, for example the $\Delta\bar{N} = f(B, S)$ variation.

Effects of sliding friction to steady state conditions in the web-roller interface

Before presenting the effects of non-dimensional parameters on traction, the steady state conditions at the tape-roller interface for a typical mixed lubrication case is presented. For this case the following values of the non-dimensional parameters were used: $B = 113.5$, $C = 1.061 \times 10^{-3}$, $P = 3.8$, $V = 1.94 \times 10^{-2}$, $\beta = \pi/2$, $\Sigma = 2 \times 10^{-2}$, $P_0 = 10$, $X_L = X_R = 1.061$, $\Lambda = 1.27$.

Figure 2 shows the steady state solution of equations (2-9) represented in terms of the non-dimensional parameters defined in equation (11). In particular, the variation of in plane stress resultant (tension) \bar{N} , tape-roller spacing \bar{h} , contact pressure \bar{p}_c and air

pressure \bar{p} are presented in the *wrap region* which spans $0 \leq \bar{x} - \bar{L}_1 \leq 1$. For this case the tape-roller spacing is less than one in the wrap region, which indicates full rigid body contact; \bar{h} varies from approximately 0.86 on the entry side ($\bar{x} = 0$) to 0.8 on the exit side. Thus it is seen that when the effects of asperity compression and in-plane stress resultant are considered no constant gap region exists in the interface. The in-plane tension \bar{N} increases approximately 40% along the interface due to sliding friction causing a subsequent increase in the belt-wrap pressure. Increasing belt-wrap pressure applies higher compression on the asperities along the interface, resulting in the variable gap height indicated above. The same effect is also responsible for the slight linear increase in contact pressure \bar{p}_c and air pressure \bar{p} .

On the exit side of the interface the air pressure shows the ondulation characteristic of the elastohydrodynamic lubrication [15,20]. This change in air pressure results in a sudden increase of the contact pressure and a sudden dip in web-roller spacing. Special care is given to the numerical resolution of the entry and exit regions: the spatial grid used in the solution has $\Delta\bar{x} = 2 \times 10^{-4}$ which results in many grid points in the transition regions.

Curve fitting

In this work two variable functions, such as $f(V_1, V_2)$, are sought to represent the variation of $\Delta\bar{N}$, where $V_1 = B$ and $V_2 \in \{S, C, P, P_0, V, \beta, \Sigma, A, \mu_s\}$. A two variable curve fitting method is developed for this. Polynomials of the following form were used,

$$\Delta\bar{N} = \sum_{i=0}^I \left(\sum_{j=0}^J D_{ij} V_2^j \right) V_1^i \quad (18)$$

The order of polynomials I and J has an upper limit of three. Curve fits for $\Delta\bar{N}$ as a function of B and V_2 are considered acceptable over a given range, provided that the maximum error does not exceed ten percent. For this reason, curve fitting is conducted using the proportional least squares regression method, which minimizes the sum of the squared percent errors.

For all cases, curve fits were obtained using $I = 1, 2$ and 3 for $\Delta\bar{N}$ as a function of B . This curve fitting is conducted for each of the 25 values of the second variable V_2 . This gives 25 different values for each of the constants D_{ij} of the polynomials. Regression is then performed on each D_{ij} , by setting $J = 1, 2$ and 3 and by using D_{ij} as a function of the second variable, V_2 . Trying different combinations of polynomials allowed flexibility in curve fitting options. In this work, most of the curve fits are reported using 3rd order polynomials in B and V_2 , i.e., $I = J = 3$. The ranges for which the maximum error is less than ten percent are reported as well as the average and maximum percent errors across the acceptance range. The success of each curve fit was evaluated based on maximum error ϵ_{max} and average error ϵ_{ave} calculated between the curve fit and the original solution for $\Delta\bar{N}$. Results are reported in V_1 and V_2 ranges where ϵ_{max} and ϵ_{min} are less than 10%.

Traction results

Variation of tension change $\Delta\bar{N}$ as a function of the bearing number B and the other nine parameters are given in Figure 3. Note again that in these plots a high value of $\Delta\bar{N}$ indicates a high traction interface. Parts a and b of Figure 3 shows that parameters V

and S do not significantly affect the change of traction $\Delta\bar{N}$ in the range of values considered. On the other hand $\Delta\bar{N}$ depends with varying degrees of strength on C , P , β , μ_s , Σ , Λ .

Figure 3a shows that in the range of V and B values considered here, $\Delta\bar{N}$ variation is independent of the non-dimensional tape speed V . A third order curve represents the data,

$$\Delta\bar{N} = 5.81 \times 10^{-1} - 1.19 \times 10^{-3} B + 1.01 \times 10^{-6} B^2 - 4.40 \times 10^{-6} B^3 \quad (19)$$

$$\text{for } 5 \times 10^{-3} \leq V \leq 5 \times 10^{-2}, \quad 14 \leq B \leq 570 \text{ and } \Delta\bar{N} > 0.1$$

with $\varepsilon_{max} = 1.30\%$ and $\varepsilon_{ave} = 0.28\%$. Total traction loss occurs near $B = 400$.

Figure 3b shows that traction change $\Delta\bar{N}$ is weakly affected by the tape-stiffness parameter S in the range of S and B values considered here. This is particularly more pronounced at lower bearing numbers B . On the other hand, complete traction loss is occurs at lower B values as the value of S becomes lower. Decreasing S values can be interpreted as decrease in tension (eqn. (12)); therefore, it is seen that traction loss occurs at a lower bearing number for lower tension values. This variation is represented by the following third order curve,

$$\begin{aligned} \Delta\bar{N} = & (5.82 \times 10^{-1} - 1.74 \times 10^{-6} S - 4.82 \times 10^{-10} S^2 + 3.63 \times 10^{-13} S^3) \\ & + (-1.20 \times 10^{-3} - 2.84 \times 10^{-8} S + 5.62 \times 10^{-11} S^2 + 1.81 \times 10^{-14} S^3) B \\ & + (1.31 \times 10^{-6} - 9.77 \times 10^{-10} S + 5.17 \times 10^{-13} S^2 - 7.07 \times 10^{-17} S^3) B^2 \\ & + (-3.87 \times 10^{-9} - 2.25 \times 10^{-12} S + 1.58 \times 10^{-15} S^2 - 4.03 \times 10^{-19} S^3) B^3 \end{aligned} \quad (20)$$

$$\text{for } 147 \leq S \leq 2467, \quad 14 \leq B \leq 570 \text{ and } \Delta\bar{N} > 0.11$$

with $\varepsilon_{max} = 8.49\%$ and $\varepsilon_{ave} = 0.89\%$.

The variation of traction as a function of the other two structural non-dimensional parameters C and P is considerably stronger. Figure 3c shows that for a given value of B traction loss is higher at high P values. This result is to be expected, as P is the non-dimensional, inverse belt-wrap pressure; thus, this result simply indicates that traction is proportional to the belt-wrap pressure. The best fit curve for this variation is as follows,

$$\begin{aligned} \Delta\bar{N} = & (5.83 \times 10^{-1} - 3.82 \times 10^{-3} P + 4.72 \times 10^{-4} P^2 + 8.85 \times 10^{-5} P^3) \\ & + (-7.22 \times 10^{-5} - 2.92 \times 10^{-4} P + 3.49 \times 10^{-5} P^2 - 9.08 \times 10^{-6} P^3) B \\ & + (-1.78 \times 10^{-7} + 4.62 \times 10^{-7} P - 3.69 \times 10^{-7} P^2 + 8.52 \times 10^{-8} P^3) B^2 \\ & + (3.79 \times 10^{-10} + 1.01 \times 10^{-9} P + 7.86 \times 10^{-10} P^2 - 2.20 \times 10^{-10} P^3) B^3 \end{aligned} \quad (21)$$

$$\text{for } 0.8 \leq P \leq 4.57, \quad 14 \leq B \leq 570 \text{ and } \Delta\bar{N} > 0.14$$

with $\varepsilon_{max} = 5.39\%$ and $\varepsilon_{ave} = 0.33\%$.

The variation of traction with the non-dimensional thickness parameter C is plotted in Figure 3d. This figure shows that the traction is higher for higher C values. This is a particularly significant finding when one considers the tape industry's need for using thinner tapes; this result indicates that it may become more difficult to achieve good traction on a given roller when thinner tapes are used. The variation shown in this figure is represented by the following curve fit,

$$\begin{aligned}
\Delta\bar{N} = & (5.35 \times 10^{-1} + 43.26C - 9026.90C^2 + 617910C^3) \\
& + (-9.38 \times 10^{-4} + 2.07 \times 10^{-1}C - 9.26C^2 + 334.07 \times 10^3 C^3)B \\
& + (-1.04 \times 10^{-6} + 1.45 \times 10^{-3}C - 4.15 \times 10^{-1}C^2 + 33.90C^3)B^2 \\
& + (-5.64 \times 10^{-10} - 3.04 \times 10^{-7}C + 1.64 \times 10^{-4}C^2 - 1.62 \times 10^{-2}C^3)B^3
\end{aligned} \tag{22}$$

$$\text{for } 1.69 \times 10^{-3} \leq C \leq 5.31 \times 10^{-3}, \quad 14 \leq B \leq 570 \quad \text{and} \quad \Delta\bar{N} > 0.19$$

with $\varepsilon_{max} = 9.74\%$ and $\varepsilon_{ave} = 0.51\%$.

The effect of β on roller traction is presented in Figure 3e. The parameter β , in equation (13a), combined with S represents the shell stiffness. This figure shows that traction is higher for higher values of β , which is not surprising given that a higher β value corresponds to a higher shell stiffness. The best fit curve to represent the effects of β and B is a third order polynomial,

$$\begin{aligned}
\Delta\bar{N} = & (5.67 \times 10^{-1} + 8.30 \times 10^{-3}\beta - 5.72 \times 10^{-5}\beta^2 - 1.51 \times 10^{-4}\beta^3) \\
& + (-2.28 \times 10^{-3} + 1.43 \times 10^{-3}\beta - 5.65 \times 10^{-4}\beta^2 + 7.93 \times 10^{-5}\beta^3)B \\
& + (-4.55 \times 10^{-7} + 7.81 \times 10^{-7}\beta - 1.18 \times 10^{-7}\beta^2 + 3.46 \times 10^{-9}\beta^3)B^2 \\
& + (-7.02 \times 10^{-9} + 4.03 \times 10^{-9}\beta - 1.47 \times 10^{-9}\beta^2 + 2.06 \times 10^{-10}\beta^3)B^3
\end{aligned} \tag{23}$$

$$\text{for } 0.408 \leq \beta \leq 3.14, \quad 14 \leq B \leq 570 \quad \text{and} \quad \Delta\bar{N} > 0.17$$

with $\varepsilon_{max} = 8.69\%$ and $\varepsilon_{ave} = 1.22\%$.

The friction coefficient μ_s effects the traction strongly. In this work the value of μ_s was varied in the 0.13 – 1.92 range. Figure 3f shows that for a given B value, higher friction coefficient results in higher traction, as expected. However, the point of total traction loss is still at $B = 400$ for all μ_s values. The data is best represented by the following mixed polynomial curve fit,

$$\begin{aligned}
\Delta\bar{N} = & (-3.24 \times 10^{-2} + 1.93\mu_s - 9.62 \times 10^{-2}\mu_s^2 + 1.12\mu_s^3) \\
& + (2.33 \times 10^{-5} - 3.21 \times 10^{-3}\mu_s + 2.65 \times 10^{-3}\mu_s^2 - 2.95 \times 10^{-3}\mu_s^3)B \\
& + (3.27 \times 10^{-7} - 4.11 \times 10^{-6}\mu_s - 6.54 \times 10^{-6}\mu_s^2 + 3.14 \times 10^{-8}\mu_s^3)B^2
\end{aligned} \tag{24}$$

$$\text{for } 0.13 \leq \mu_s \leq 1.92, \quad 30 \leq B \leq 371 \quad \text{and} \quad \Delta\bar{N} > 0.2$$

with $\varepsilon_{max} = 8.72\%$ and $\varepsilon_{ave} = 1.50\%$.

The effect of non-dimensional asperity engagement height Σ on traction is presented in Figure 3g. This figure shows that for low values of Σ traction remains high as B increases. This is the only counterintuitive artifact of the non-dimensionalization used here. In order to explain this result note in equation (11) that A , Σ and B all include the dimensional asperity height σ_o in their definitions. In order to keep A and B unaffected from variations of Σ , as σ_o increases the physical values of λ and μ_a need to be increased, respectively; hence, for higher Σ values higher air pressure is generated; this causes the traction to be higher for lower Σ . Variation of traction with Σ is quite strong and is represented by the following third order polynomial fit,

$$\begin{aligned}
\Delta\bar{N} = & (5.74 \times 10^{-1} + 7.97 \times 10^{-1} \Sigma - 14.44 \Sigma^2 + 106.75 \Sigma^3) \\
& + (-4.02 \times 10^{-4} - 9.06 \times 10^{-2} \Sigma + 1.36 \Sigma^2 - 9.96 \Sigma^3) B \\
& + (-7.49 \times 10^{-7} + 2.03 \times 10^{-4} \Sigma - 2.32 \times 10^{-3} \Sigma^2 + 1.15 \times 10^{-2} \Sigma^3) B^2 \\
& + (1.70 \times 10^{-9} - 4.78 \times 10^{-7} \Sigma - 1.72 \times 10^{-5} \Sigma^2 + 1.58 \times 10^{-4} \Sigma^3) B^3
\end{aligned} \tag{25}$$

$$\text{for } 5.18 \times 10^{-3} \leq \Sigma \leq 6 \times 10^{-2}, \quad 14 \leq B \leq 570 \quad \text{and} \quad \Delta\bar{N} > 0.1$$

with $\varepsilon_{max} = 9.84 \%$ and $\varepsilon_{ave} = 1.1 \%$.

The effect of non-dimensional contact stiffness P_o of asperities is plotted in Figure 3h. In order to obtain this variation, P_o was varied three orders of magnitude, $10^2 - 10^5$. This figure shows that traction is higher for stiffer asperities. However, the effect of asperity stiffness saturates quickly after $P_o = 3 \times 10^4$. The dependence of traction on asperity stiffness and bearing number is represented with the following third order polynomial fit,

$$\begin{aligned}
\Delta\bar{N} = & (6.15 \times 10^{-1} + 4.33 \times 10^{-7} P_o - 8.16 \times 10^{-12} P_o^2 + 4.58 \times 10^{-17} P_o^3) \\
& + (-1.33 \times 10^{-3} - 1.35 \times 10^{-9} P_o + 2.30 \times 10^{-14} P_o^2 - 1.22 \times 10^{-19} P_o^3) B \\
& + (3.00 \times 10^{-6} + 2.98 \times 10^{-11} P_o - 5.45 \times 10^{-16} P_o^2 + 3.02 \times 10^{-21} P_o^3) B^2 \\
& + (-8.37 \times 10^{-9} - 5.68 \times 10^{-14} P_o + 1.04 \times 10^{-18} P_o^2 - 5.73 \times 10^{-24} P_o^3) B^3
\end{aligned} \tag{26}$$

$$\text{for } 10^2 \leq P_o \leq 10^5, \quad 14 \leq B \leq 570 \quad \text{and} \quad \Delta\bar{N} > 0.13$$

with $\varepsilon_{max} = 9.20 \%$ and $\varepsilon_{ave} = 1 \%$.

The effect of non-dimensional molecular mean free path Λ is shown in Figure 3i. This variable was tested in the range 0.8 – 6.35. This figure shows that if the non-dimensional molecular mean free path length is higher the traction remains higher for a wider range of B values; this indicates that in the mixed lubrication problem less air pressure would be developed in the interface. The following third order polynomial fit represents the variation,

$$\begin{aligned}
\Delta\bar{N} = & (5.73 \times 10^{-1} + 1.95 \times 10^{-3} \Lambda + 2.39 \times 10^{-4} \Lambda^2 - 3.78 \times 10^{-5} \Lambda^3) \\
& + (-1.58 \times 10^{-3} + 5.52 \times 10^{-4} \Lambda - 9.32 \times 10^{-5} \Lambda^2 + 5.78 \times 10^{-6} \Lambda^3) B \\
& + (-5.74 \times 10^{-8} + 1.57 \times 10^{-7} \Lambda - 3.48 \times 10^{-8} \Lambda^2 + 2.23 \times 10^{-9} \Lambda^3) B^2 \\
& + (-4.01 \times 10^{-9} + 1.97 \times 10^{-9} \Lambda - 3.49 \times 10^{-10} \Lambda^2 + 2.13 \times 10^{-11} \Lambda^3) B^3
\end{aligned} \tag{27}$$

$$\text{for } 1.49 \leq \Lambda \leq 6.35, \quad 43 \leq B \leq 570 \quad \text{and} \quad \Delta\bar{N} > 0.196$$

with $\varepsilon_{max} = 7.43 \%$ and $\varepsilon_{ave} = 1.01 \%$.

Summary and Conclusions

A comprehensive model for predicting traction of an impermeable web over a non-grooved roller is introduced. In the model the web is modeled at steady state with a tensioned Euler-Bernoulli beam. The change of tension due to relative slip between the roller and the web is modeled by considering in-plane equilibrium of the stress resultants and Coulomb's law of friction. The effect of air lubrication is modeled with Reynolds

lubrication equation with first order slip-flow corrections. The rigid body contact between the asperities is modeled using the empirically based asperity compliance curve. The problem is non-dimensionalized and twelve non-dimensional parameters are identified. The effects of ten of these non-dimensional parameters on the traction between the web and the roller are investigated numerically. Results are presented in graphs and in the forms of two variable polynomial curve fits. It was shown that dependence of traction on the non-dimensional transport velocity V and stiffness parameter S are weak; but traction depends on the other eight parameters strong as shown in equations (19-27). The results can be used by tape path designers to predict traction.

References

- [1] Ducotey, K. S. and Good, J. K., 1999, "Predicting traction in web handling," *Journal of Tribology, Trans ASME*, **121**, pp. 618-624.
- [2] Rice, B., Cole, K.A. and Müftü, S., 2002, "A model for determining the asperity engagement height in relation to web traction over non-vented rollers," *Journal of Tribology, Trans ASME*, **124**(3), pp. 584-594.
- [3] Johnson, K.L., 1985, *Contact Mechanics*, p. 245, Cambridge University Press
- [4] Eshel, A. and Elrod, H.G., 1965, "Theory of infinitely wide, perfectly flexible, self acting foil bearing," *J. Basic Engineering*, Dec., pp. 831-836.
- [5] Stahl, K.J., White, J.W. and Deckert, K.L., 1974, "Dynamic response of self acting foil bearings," *IBM Journal of Research and Development*, pp. 513-520.
- [6] Rongen, P. M. J., 1994, *Finite Element Analysis of the Tape Scanner Interface in Helical Scan Recording*, Ph.D. thesis, Technische Univesiteit Eindhoven, The Netherlands.
- [7] Hashimoto, H., 1999, "Air film thickness estimation," *Journal of Tribology, Trans ASME*, **121**, pp. 50-55.
- [8] Lakshmikumaran, A. and Wickert, J.A., 1998, "Equilibrium analysis of finite width tension dominated foil bearings," *Journal of Tribology, Trans ASME*, **121**, pp. 108-113.
- [9] Lacey, C. and Talke, F., 1992, "Measurement and simulation of partial contact at the head/tape interface," *Journal of Tribology, Trans ASME*, **144** pp. 646-652.
- [10] Wu, Y., Talke, F., 1996, "The Effect of Surface Roughness on the Head-tape Interface", *Journal of Tribology, Trans ASME*, **118**(2), pp. 376-381.
- [11] Müftü, S. and Benson, R.C, 1996, "A study on width-wise variations in the two dimensional foil bearing problem", *Journal of Tribology*, **118**, pp. 407-414.
- [12] Müftü, S. and Kaiser, D.J., 2000, "Measurements and theoretical predicitions of the head/tape spacing over a flat-head," *Tribology International*, **33**, pp. 415-430.
- [13] Ducotey, K. S. and Good, J. K., 2000, "A numerical algorithm for determining the traction between a web and a circumferentially grooved roller," *Journal of Tribology, Trans ASME*, **122**, pp. 578-584.
- [14] S. Müftü and R.C. Benson, 1995, "Modelling the Transport of Paper Webs Including the Paper Permeability Effects," *Proceedings of the I.S.P.S., ASME International Congress and Exposition, San Francisco, CA, November 1995*, pp. 247-258.
- [15] Müftü, S. and Altan, M.C., 1999, "Mechanics of a Porous Web Moving Over a Cylindrical Guide," *Journal of Tribology, Trans ASME*, **122**, pp. 418-426.
- [16] Hashimoto, H., 1997, "Effects of foil bending rigidity on spacing height characteristics of hydrostatic porous foil bearings for web handling processes," *Journal of Tribology, Trans ASME*, **119**, pp. 422-427.
- [17] Müftü, S. and Cole, K.A., 1999, "The Fluid/Structure Interaction of a Thin Flexible Cylindrical Web Supported by an Air Cushion," *J. Fluids and Struc.*, **13**, pp. 681-708.
- [18] Kikuchi N. and Oden, T.J., 1988, *Contact Problems in Elasticity*, Ch. 9, SIAM, Philadelphia, PA.
- [19] Burgdorfer, A., 1959, "The influence of molecular mean free path on the performance of hydrodynamic gas lubricated bearings," *Journal of Basic Engineering, Trans ASME*, March, pp. 94-100.
- [20] Gross, W.A., ed., 1980, *Fluid Film Lubrication*, John Wiley and Sons, New York, Chapter 6.

E	5 GPa	μ_s	0.3
ν	0.3	σ_0	50 nm
c	5 μm	p_0	1.013 MPa
ρ	1500 kg/m ³	λ	63.5 nm
T	80 N/m	μ_a	1.85×10 ⁻⁵ Pa.s
v_w	2 m/s	P_a	101.3 kPa
R	3 mm		
β	90°		

Table 1 The values of the parameters for a typical modern tape drive application.

S	343	Σ	1×10 ⁻²
C	1.06×10 ⁻³	P_0	10
V	1.94×10 ⁻²	B	4129
P	3.8	Λ	1.27
β	1.57	μ_s	0.3
X_L, X_R	1.06		

Table 2 Values of the non-dimensional parameters corresponding to the values given in Table 1.

S	148 – 2470	Σ	7×10 ⁻⁴ – 2×10 ⁻²
C	2.12×10 ⁻⁴ – 5.31×10 ⁻³	P_0	10 ² -10 ⁵
V	5×10 ⁻³ – 0.025	B	14-570
P	0.84 – 25	Λ	0.8–6.35
β	0.28 – 3.14	μ_s	0.05–2
X_L, X_R	1.06		

Table 3 Ranges of the non-dimensional parameters used in the analysis.

Nomenclature

Dimensional parameters

b	Bending length of the web $(D/T)^{1/2}$
c	Web thickness
D	Bending rigidity of web, $Ec^3/12(1-\nu^2)$
D_s	Shell stiffness of the web, $Ec/R^2(1-\nu^2)$
E	Elastic modulus of the web
F_f	Friction force
F_n	Normal force due to rigid body contact
H	Heaviside step function
L_1, L_2	Tangency points of the web
L_w	Wrap length (L_2-L_1)
N	In-plane stress resultant
p	Air pressure
p_c	Contact pressure
p_0	Asperity compliance
P_a	Ambient air pressure
R_r	Roller radius
$R(x)$	Radius of curvature of the web
T	Web tension per width
v_w	Web transport speed
w	Web displacement normal to its surface
w'	Web displacement relative w_r
w_r	Equilibrium clearance
x_b, x_r	Length of unwrapped web
β	Web wrap angle
λ	Mean free path length for air
μ_a	Air viscosity
μ_s	Friction coefficient at very slow speeds
μ_e	Equivalent friction coefficient due to air entrainment
μ	Static friction coefficient
ν	Poisson's ratio
ρ	Web mass density
σ_o	Asperity contact height
τ	In plane traction

Non-dimensional parameters

B	Bearing number
C	Thickness
P	Belt-wrap pressure
P_0	Asperity compliance
S	Stiffness parameter
V	Transport velocity
Λ	Mean free path of air
Σ	Asperity contact height
X_L, X_R	Length of unwrapped web

List of Figure Captions

Figure 1 Schematic representation of a web moving over a roller at the onset of sliding.

Figure 2 Variation of non-dimensional tension \bar{N} , tape-roller spacing \bar{h} , contact pressure \bar{p}_c and air pressure \bar{p} in the *wrap region* which spans $0 \leq \bar{x} - \bar{L}_1 \leq 1$. $B = 113.5$, $C = 1.061 \times 10^{-3}$, $P = 3.8$, $V = 1.94 \times 10^{-2}$, $\beta = \pi/2$, $\Sigma = 2 \times 10^{-2}$, $P_o = 10$, $X_L = X_R = 1.061$, $A = 1.27$. The tape moves from left to right in this figure.

Figure 3 The effect of the parameters B , V , S , C , P , μ_s , β , Σ , P_o and A on traction in the web roller interface. Unless otherwise specified on the figures the values of the variables are given in Table 2.

List of Table Captions

Table 1 The values of the parameters for a typical modern tape drive application.

Table 2 Values of the non-dimensional parameters corresponding to the values given in Table 1.

Table 3 Ranges of the non-dimensional parameters used in the analysis.

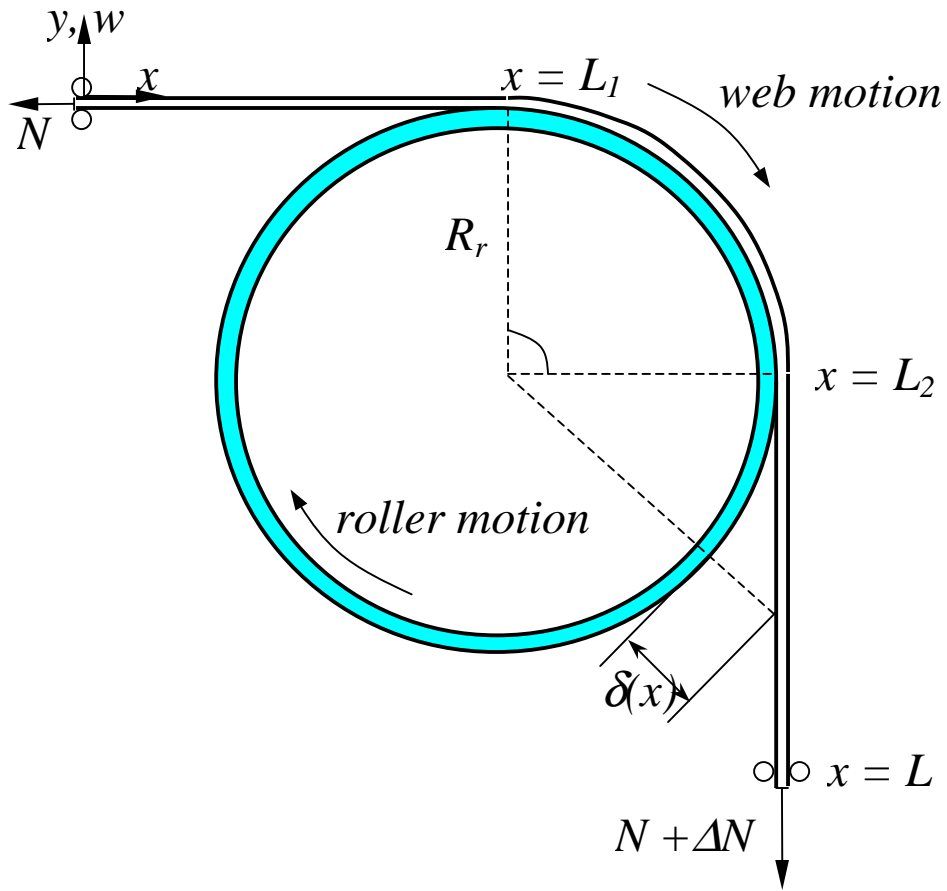


Figure 1 Schematic representation of a web moving over a roller at the onset of sliding.

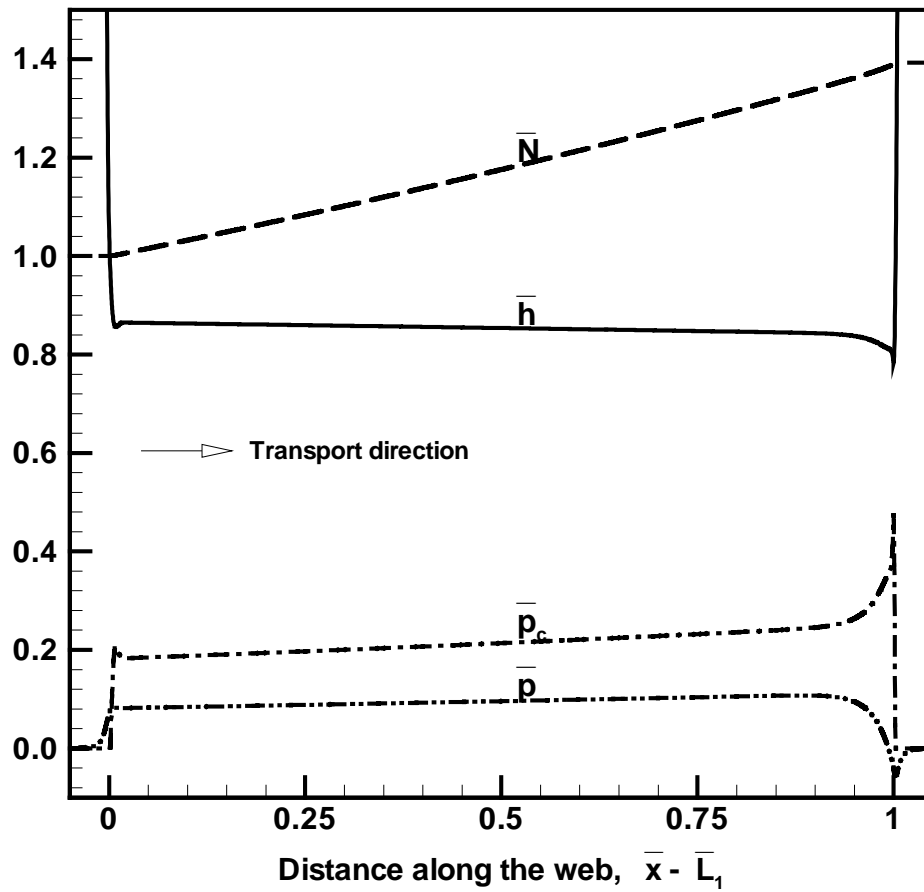
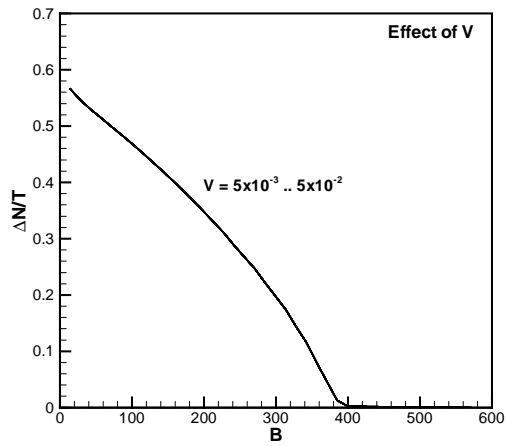
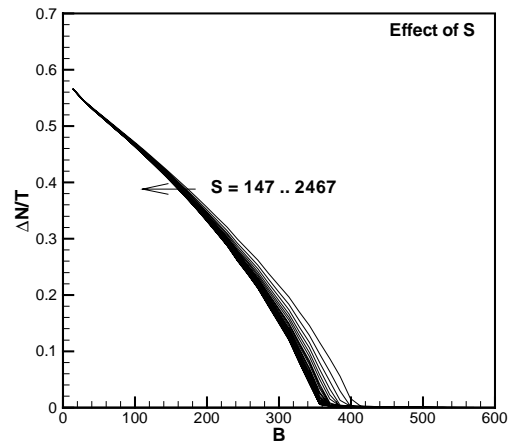


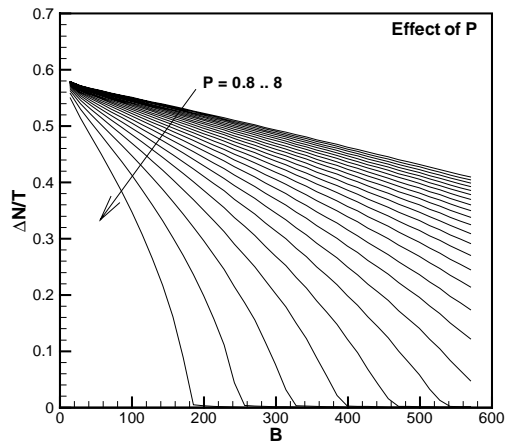
Figure 2 Variation of non-dimensional tension \bar{N} , tape-roller spacing \bar{h} , contact pressure \bar{p}_c and air pressure \bar{p} in the *wrap region* which spans $0 \leq \bar{x} - \bar{L}_1 \leq 1$. $B = 113.5$, $C = 1.061 \times 10^{-3}$, $P = 3.8$, $V = 1.94 \times 10^{-2}$, $\beta = \pi/2$, $\Sigma = 2 \times 10^{-2}$, $P_o = 10$, $X_L = X_R = 1.061$, $A = 1.27$. The tape moves from left to right in this figure.



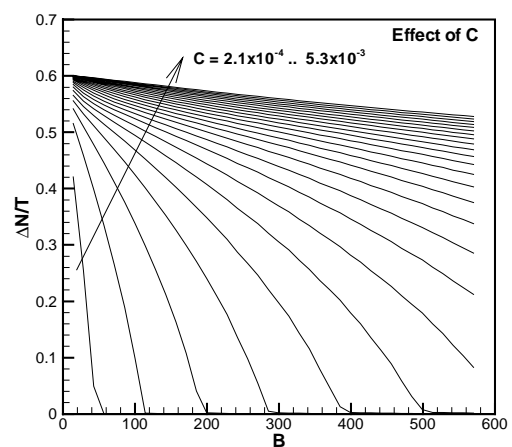
a)



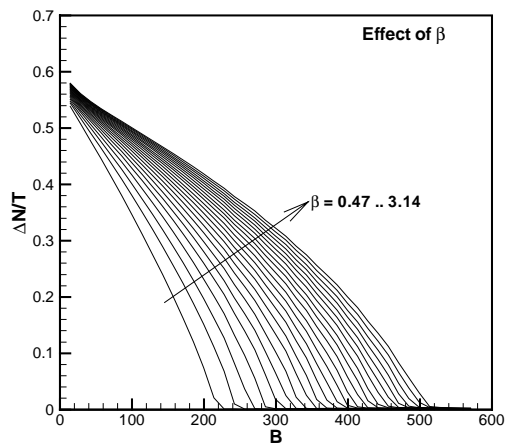
b)



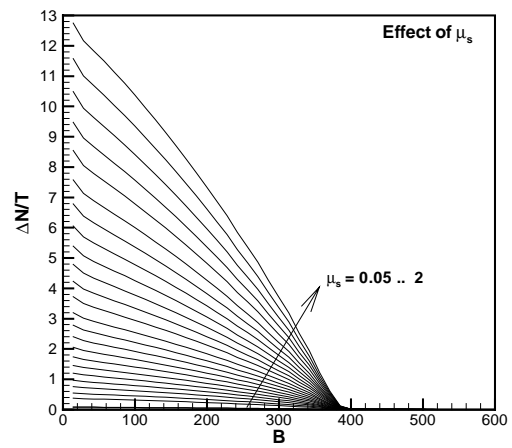
c)



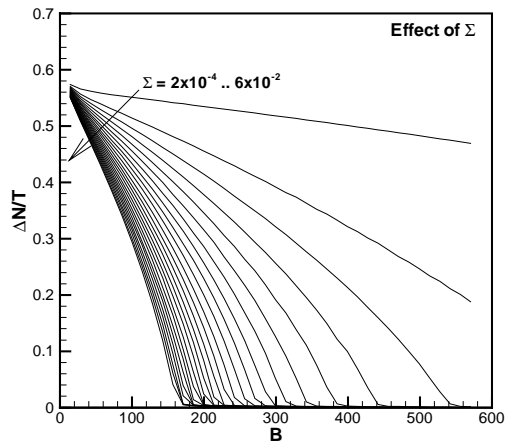
d)



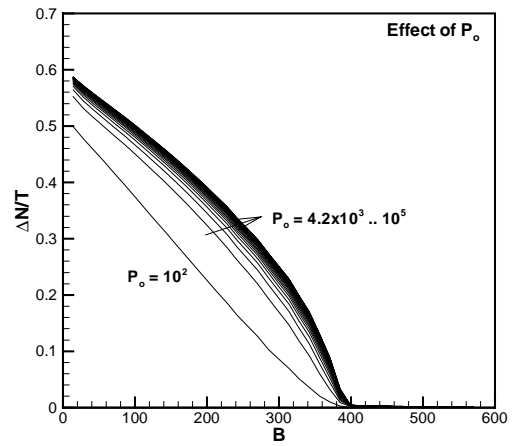
e)



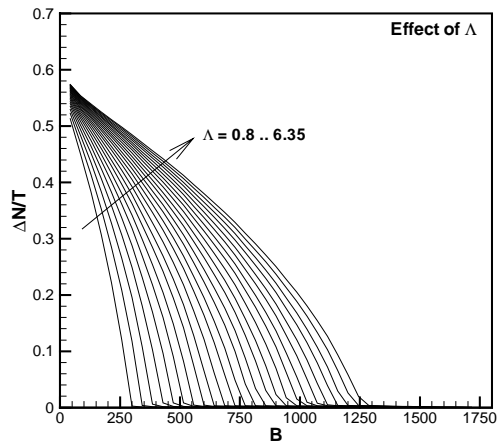
f)



g)



h)



i)

Figure 3 The effect of the parameters B , V , S , C , P , μ_s , β , Σ , P_o and Λ on traction in the web roller interface. Unless otherwise specified on the figures the values of the variables are given in Table 2.